PROCEEDINGS, Fire and Evacuation Modeling Technical Conference (FEMTC) 2024
Kansas City, Missouri, September 18-20, 2024

Convective Heat Transfer from Impinging Flames

Jonathan L. Hodges
Jensen Hughes
Blacksburg, Virginia, USA
email: jhodges@jensenhughes.com

Randall J. McDermott
National Institute of Standards and Technology
Gaithersburg, Maryland, USA
email: randall.mcdermott@nist.gov

ABSTRACT

Convective heat transfer in the Fire Dynamics Simulator (FDS) software is based on empirical relationships for natural and forced convection. The forced convection relationship typically dominates the convective heat transfer from a fire to a wall or ceiling in the near-field due to the magnitude of the velocity being generated by the plume. Cases where the fire directly impinges on the surface lead to low forced convection heat transfer coefficients due to the local stagnation point. This results in a local minimum in the convective heat transfer coefficient where FDS transitions from a forced convection relationship to a natural convection relationship. However, this behavior is not seen in experiments where the peak heat transfer from an impinging fire is at the stagnation point. To address this problem, in this paper we implement an impinging jet heat transfer relationship in FDS, utilizing the stagnation pressure to form the velocity scale. Heat flux predictions from FDS are compared with experimental data on an impinging ceiling from two test series including thirteen experiments using the default and impinging jet models. The downstream impacts of these differences on the heating of a structural element are subsequently evaluated with a lumped capacitance thermal model.

INTRODUCTION

Convective heat transfer in the Fire Dynamics Simulator (FDS) software is based on empirical relationships for natural and forced convection [22]. The forced convection relationship typically dominates the convective heat transfer from a fire to a wall or ceiling in the near-field due to the magnitude of the buoyant velocity being generated by the plume. Cases where the fire directly impinges on the surface lead to low forced convection heat transfer coefficients due to the local stagnation point. This results in a local minimum in the convective heat transfer coefficient where FDS transitions from a forced convection relationship to a natural convection relationship, as shown in Figure 1 (see the configurations section for a description of the case). However, this behavior is not seen in diffusion flame experiments where the peak heat transfer from an impinging fire is at the stagnation point [11, 14].

This paper presents the adaptation of an existing impinging jet heat transfer relationship and its

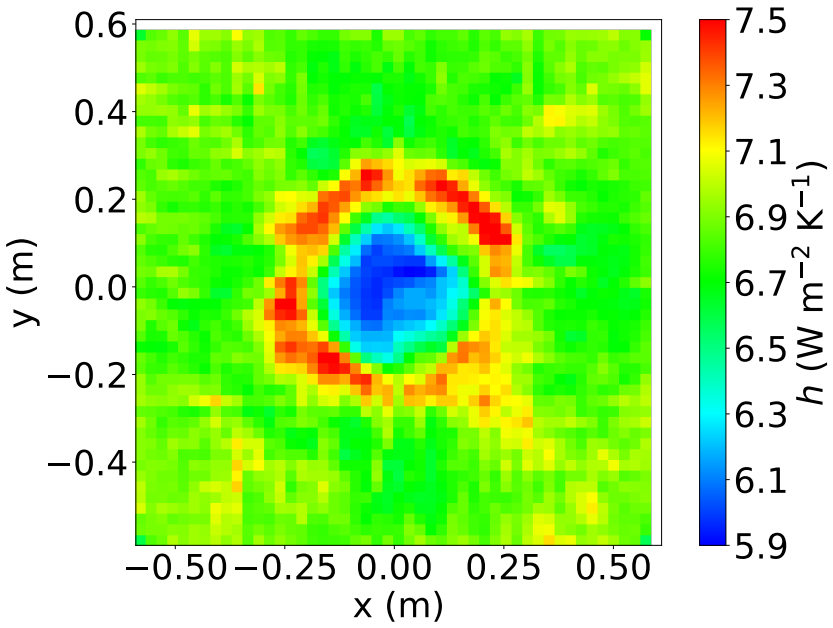

Figure 1: Heat transfer coefficient from a 90 kW fire impinging on a ceiling located 0.64 m above the fire using the default FDS convection configuration. No ambient flow biasing.

implementation in FDS. Heat flux predictions from FDS are compared with experimental data on an impinging ceiling from two test series including thirteen experiments. The heat fluxes predicted using the new model are compared with those using the default model and experimental measurements in each configurations. The downstream impacts of these differences on the heating of a structural element are subsequently evaluated with a lumped capacitance thermal model to demonstrate the potential impact of this change in a performance-based design (PBD) application.

PERFORMANCE-BASED DESIGN

There has been an increase in the use of FDS to support performance-based design (PBD) in recent years. One such application of PBD is to evaluate the need for passive fire protection coatings on structural members. The international building code (IBC) requires minimum fire resistance ratings depending on the required building construction type (e.g., 3-hour rating for Type 1A construction such as a residential high-rise building [6]). These fire resistance ratings are established by standard testing [7] such as ASTM E119 [2] or UL 263 [26]. Passive fire protection is often necessary to achieve the fire resistance ratings for structural elements required by the IBC. However, the prescriptively required fire resistance ratings may be overly conservative in some scenarios as they do not consider the variation in potential fire hazards. The IBC allows for a performance-based solution in §703.2.3 and §104.2.3.4 as long as the alternative method provides an equivalent level of safety to the prescriptive solution.

One alternative method is to use computer models to evaluate the performance of structural elements to realistic design fires. In this approach, a CFD fire model such as FDS is first used to characterize the thermal exposure to structural elements. These exposures can then be used as a boundary condition in a detailed thermal model of the element to determine the distribution of heat through the material. An equivalent level of safety is achieved if the model-predicted strength of the

element exceeds that of an element under the standard exposure with the prescriptively-required fire resistance rating. A typical failure criteria for steel members is a section average temperature of 538 °C for columns due to a 50% reduction in stiffness and 593 °C for beams due to a 50% reduction in yield strength.

This approach relies on the accuracy of the heat transfer predictions in the CFD fire model. While the majority of the heat transfer is often through radiation due to the fourth power dependence with flame temperature, convective heat transfer can be significant when a fire is in direct contact with a surface. The Society of Fire Protection Engineers (SFPE) recommends a convective heat transfer coefficient of 30 W/(m^2 K) [25] for surfaces exposed to realistic fires; however, the default convection relationships in FDS rarely predict values higher than 15 W/(m^2 K).

METHODOLOGY

Predictions of the heat transfer using the impinging jet model are compared with existing Nusselt relationships and several experiments in this study. The impinging jet relationship and the experiments with a diffusion flame impinging on an unconfined ceiling were used to tune the Nusselt relationships, and the two other studies were used to evaluate the model performance. The following subsections provide a high level description of these configurations.

Impinging Jet Heat Transfer

Impinging jet flow poses a challenge for convective heat transfer models because the stagnation velocity goes to zero numerically near the mean stagnation point and hence the computed Reynolds number is fictitiously low leading to an under-prediction of the local heat transfer coefficient. The form of the impinging jet model is similar to a forced convection correlation but the Reynolds number is computing using an "impact velocity", U_{imp}, derived from the stagnation pressure, following the method proposed by Huang [16]. The stagnation energy per unit mass, H, is used as the stagnation pressure in this method, and is defined as

$$H \equiv |\mathbf{u}|^2/2 + \tilde{p}/\rho \tag{1}$$

where $\mathbf{u}$ is the velocity, $\tilde{p}$ is the perturbation pressure, and ρ is the fluid density. The velocity scale is defined as

$$U_{\text{imp}} = \sqrt{2H}. \tag{2}$$

The Reynolds number is computed using the equation

$$\text{Re}_{\text{imp}} = \frac{\rho_\infty U_{\text{imp}} D}{\mu_\infty} \tag{3}$$

where μ is the fluid dynamic viscosity, D is the fire diameter, and the subscript ∞ indicates the properties are calculated based on ambient properties at the inlet (i.e., burner surface).

We take our target correlation to be that of Martin [18, 3] where the Nusselt number is calculated using the equation

$$\text{Nu}_{\text{imp}} = C_0 + \left(C_1 \,\text{Re}_{\text{imp}}^m - C_2\right)\, \text{Pr}^{1/3} \tag{4}$$

where Pr is the Prandtl number, C_n and m are coefficients. The default coefficients are $C_0 = 0$, $C_1 = 0.021$, $C_2 = 0$, $m = 0.8$ which were selected by comparing with existing correlations and

experiments (see the configurations section for a discussion of tuning coefficients). The heat transfer coefficient is calculated from the Nu using the equation

$$h = \frac{k_{\text{film}}}{D}\text{Nu}_{\text{imp}} \tag{5}$$

where h is the heat transfer coefficient, and k_{film} is the fluid thermal conductivity at the film temperature.

Configurations

Non-Reacting Hot Jet

The coefficients in Eq. 4 were tuned by comparing with the correlation presented by Martin [3, 18]. The set up for the problem is a simple cubic domain 1 m on a side. The lateral boundaries are open except for the ceiling which is isothermal at 20 °C. A hot jet of air is injected from a 0.2 m by 0.2 m square vent at 100 °C. Two Reynolds numbers are considered by changing the inlet flow velocity from 10-40 m/s. Three grid resolutions for each Reynolds number are tested, $D/\delta x$ = 7, 14, 28, representing *coarse*, *medium*, and *fine* resolutions. The cases are run for roughly ten flow through times with statistics collected over the last half of the simulation. The convection heat transfer predicted by FDS using U_{imp} is compared with the values predicted by the original correlation based on the inlet velocity.

Fire Impinging on an Unconfined Ceiling

Wasson studied the split between convection and radiation heat transfer from a diffusion flame impinging on a ceiling [27] using the apparatus shown in Fig. 2. The ceiling was 1.2 m square with an adjustable ceiling height. The author used a 0.3 m square 0.15 m tall propane burner with 50 kW and 90 kW HRRs. The ceiling placement was varied to investigate the impact of different flame length to height ratios on the measured heat transfer rates. The experiments conducted by Wasson are shown in Table 1. Ceiling height, H, is the height between the top of the burner and the bottom of the ceiling.

Heat fluxes at the stagnation point were measured using a high temperature hybrid heat flux gauge which operates as both a thermopile and a slug calorimeter [8]. The author measured gas temperatures near the heat flux gauge using an aspirated thermocouple. The heat transfer coefficient was calculated by the author using four different approaches utilizing multiple heat flux gauges and gas temperature measurements. The heat fluxes measured by the author were not water cooled, and thus measured the net heat flux into the gauge which is a function of the gauge temperature. These values were converted to a water cooled heat flux for comparison in this analysis using the equation

$$\dot{q}''_{\text{tot,g}} = \dot{q}''_{\text{net}} + \sigma\left(T^4_{\text{gauge}} - T^4_{\infty}\right) + h\left(T_{\text{gauge}} - T_{\infty}\right) \tag{6}$$

where $\dot{q}''_{\text{tot,g}}$ is the gauge heat flux, $\dot{q}''_{\text{net}}$ is the measured net heat flux, σ is the Stefan-Boltzmann constant, T_{gauge} is the gauge temperature, and T_∞ is the reference temperature of the water cooled gauge (20 °C in this work). The heat transfer coefficients for each configuration were taken to be the median of the four methods across testing. Table 1 summarizes the heat fluxes, gas temperatures, and heat transfer coefficients from this test series. Scenario 5 was omitted from benchmarking in this work due to high transience observed in the test data.

Table 1: Wasson fire impinging on an unconfined ceiling experiments.

Test	HRR (kW)	H (m)	h (W/m^2 K)	$\dot{q}''_{\text{tot,g}}$ (kW/m^2)	T_{gas} (°C)
1	50	0.97	34.8	13.9	296.8
2	50	0.64	36.1	35.7	550.6
3	50	0.49	50.5	56.9	676.5
4	90	1.28	42.0	23.1	396.3
5*	90	0.85	60.8	56.3	682.5
6	90	0.64	57.5	75.8	839.4

*Omitted due to high transience in testing.

Figure 2: Wasson fire impinging on an unconfined ceiling [27].

Fire Impinging on a Corridor Ceiling

Lattimer *et al.* studied the thermal environment created by a fire impinging on a ceiling at the end of a corridor in [15]. The apparatus, shown in Figure 3, consisted of a 2.4 m long 1.2 m wide corridor with a ceiling height of 2.1 m from the floor. The back wall and back 1.2 m of the side walls extended 1.2 m below the ceiling. The remaining 1.2 m of the side walls were extended 0.6 m below the ceiling. The overall apparatus was elevated 0.9 m off of the floor to allow air to flow into the bottom of the corridor from all sides. A 0.46 m deep by 1.15 m wide propane sand burner was centered on the back wall with the top surface located either 0.6 m or 1.1 m from the ceiling. Each separation distance was tested at four heat release rates ranging from 100-400 kW.

The authors measured the water cooled gauge heat flux and gas temperature at four locations along the ceiling. The distances from the back wall were 0.3 m, 0.9 m, 1.5 m, and 2.1 m. Table 2 summarizes the test conditions and measurements from this test series.

Table 2: Lattimer fire impinging on a corridor ceiling experiments.

Test	HRR (kW)	H (m)	$\dot{q}''_{tot,g}$ (kW/m^2)				T_{gas} (°C)			
			0.3 m	0.9 m	1.5 m	2.1 m	0.3 m	0.9 m	1.5 m	2.1 m
1	150	1.1	26.4	17.2	8.9	7.0	400	354	312	270
2	200	1.1	39.0	24.3	12.5	9.7	507	444	389	332
3	300	1.1	74.0	43.9	23.5	17.4	736	633	545	458
4	400	1.1	108.6	62.9	32.6	22.7	887	770	641	529
5	100	0.6	31.3	15.3	7.7	6.7	494	426	355	290
6	200	0.6	75.3	36.2	18.5	13.3	800	658	532	432
7	300	0.6	124.3	66.3	31.0	16.7	1026	849	659	527
8	400	0.6	152.5	82.1	47.3	27.4	1144	973	788	630

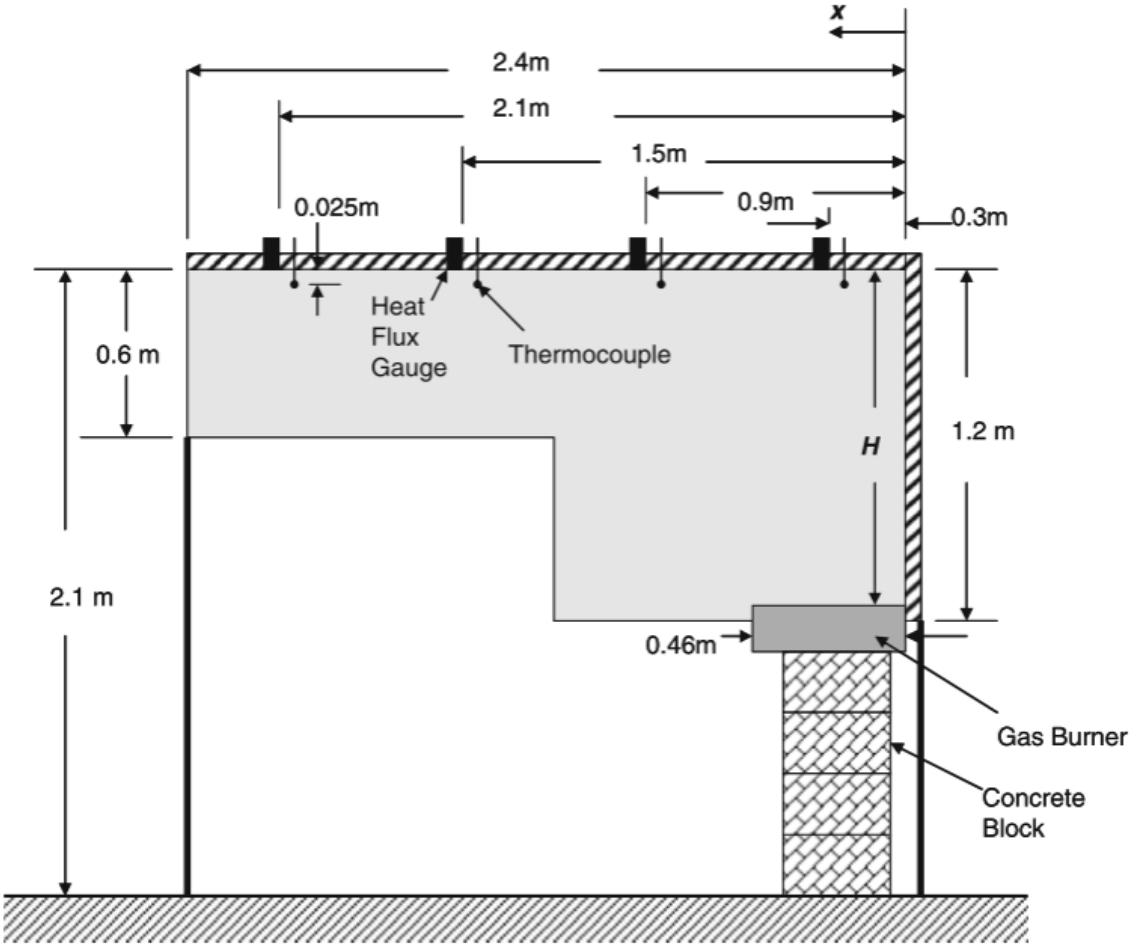

Figure 3: Lattimer fire impinging on a corridor ceiling experiments [15].

Fire Dynamics Simulator (FDS)

Fire Dynamics Simulator (FDS) is a open source CFD program developed to support modeling of fires and fire driven flows in the built environment [20]. All CFD fire models presented in this section used Fire Dynamics Simulator (FDS, version 6.9.1 commit *0beeb1f6*) unless otherwise noted. All parameters were set as the default values unless otherwise specified in the individual sections. The following sub-sections provide an overview of the specific sub-modules in FDS where non-default parameters are used in this work. Full details can be found in the freely available model documentation at http://pages.nist.gov/fds.

Turbulence Model

This work utilized the non-default large eddy simulation (LES) simulation mode which is designed for finer grid simulations and grid convergence studies. This mode switches to a convergent flux limiter scheme, CHARM [29], and a more restrictive velocity norm in the calculation of the simulation time step.

Convective Heat Transfer

In an LES calculation, a subgrid model is needed to predict convection heat transfer since the boundary layer near the wall is not resolved. FDS contains a number of different correlations for computing the heat transfer coefficient to surfaces. The default approach used in FDS is to compute a natural and a forced convection heat transfer coefficient using flat plate heat transfer correlations where FDS picks the larger value from the two correlations.

This paper compares predictions with the default FDS forced convection model and a newly implemented impinging jet convection model discussed in impinging jet section. When the impinging jet model is active, the heat transfer coefficient obtained from $\mathrm{Nu}_{\mathrm{imp}}$ is compared to that from forced and free convection and the largest value is chosen for the surface.

Radiation Heat Transfer

FDS uses a finite volume method for predicting radiation transport [12]. This is a control volume approach which divides the unit sphere into a number of solid angles. The number of radiation angles was increased to 400 in this work to reduce the potential for mesh artifacts in the discretization [13]. The number of time steps between updates to the radiation equation was increased from the default 3 to 12 to maintain the same computational time for the radiation solver at the higher spatial resolution.

Combustion Model

The combustion model used in this analysis was a two-step, mixing-controlled combustion scheme. In this model, the reaction is assumed to occur infinitely fast, which means whenever gaseous fuel and oxygen are present and mixed in the same grid cell, they are assumed to react instantly until either the fuel is consumed or oxygen concentration in the cell reaches the lower flammability limit. The first step of the reaction converts 2/3 of the carbon atoms in the fuel molecule into CO and the rest into soot. The second step oxidizes CO and soot to CO_2 to achieve the user defined post-flame yields of CO and soot. The gas phase reaction was propane, C_3H_8, with a soot yield of 0.024, carbon monoxide yield of 0.005 [24], for the Wasson and Lattimer cases. All other parameters used the default values in FDS.

FDS can be used to predict piloted and unpiloted ignition through the use of an autoignition temperature. A mixed approach was used in this work where 1% of the fuel at the burner was considered a pilot fuel with an auto ignition temperature of 0 °C and the remaining fuel had a specified auto ignition temperature of 450 °C for propane [4].

By default, FDS will invoke a gas phase flame extinction model based on the local oxygen concentration and cell temperature. This model was disabled in this work.

Model Configuration

Fuel Surface

The sand burner in each experiment was modeled as a single rectangular cuboid with no lip located below the ceiling. The top of the fuel surface was defined as a prescribed heat release rate per unit area with a 10% random perturbation in the mass flux of fuel across the surface. The front surface temperature of the burner was set to 400 °C based on data collected from a similar fire size in the Jensen Hughes laboratory.

Boundary Conditions

The Wasson unconfined ceiling cases used open boundaries for the top and sides of the domain with ambient wind along one axis as discussed in the dynamic pressure section. The floor was modeled as 0.1 m concrete with a density of 2,000 kg/m^3, specific heat of 0.9 kJ/(kg K), thermal conductivity of 1.0 W/(m K), and an emissivity of 0.9. The ceiling was modeled as 0.0159 m thick gypsum wallboard with a density of 711 kg/m^3, thermal conductivity of 0.17 W/(m K), and an emissivity of 0.9. The nominal specific heat capacity of the gypsum was 1.05 kJ/(kg K); however, temperature dependent values were used at less than 200 °C to account for the effects of decalcination [10]. The function was generally triangular with an initial growth at 80 °C to a peak of 12.86 kJ/(kg K) at 106 °C and majority of the drop occurring by 160 °C.

The Lattimer corridor cases used open boundaries for the tops and sides with no ambient wind. The floor and concrete blocks were modeled as 0.1 m concrete with the same properties as the Wasson case. The walls and ceilings of the corridor and sides of the burner were modeled as ceramic fiber blanket with a density of 96 kg/m^3, specific heat of 1.14 kJ/(kg K), thermal conductivity of 0.14 W/(m K), and an emissivity of 0.9 [9].

Meshing

Fully resolving the mechanics of a reacting fluid flow requires grid resolutions on the order of 1 mm which is impractical for engineering applications. FDS has different empirical models to improve the convergence at coarser grid resolutions. However, grid independence within the fire plume at coarse resolutions is still difficult due to the uncertainties in the different empirical formulations used in the model.

A hybrid meshing strategy was used in the Wasson cases which were used for the grid convergence study in this work, as shown in Figure 4. A finer mesh was used in the region surrounding the ceiling and fire, with a coarser mesh with a fixed resolution of 50 mm used for a larger region. In each case the coarse mesh extended an additional 0.5 m in the lateral directions. The top of the mesh was approximately 0.5 m above the ceiling; however, this varied slightly as the vertical resolution was selected such that the distance between the top of the burner and the ceiling exactly

matched the values reported in the experiment. The extent of the fine mesh above the ceiling was selected such that the number of cells were evenly divisible by 16 to facilitate splitting the mesh for MPI processing. The thickness of the ceiling in the gas phase was fixed at one grid cell of the fine mesh.

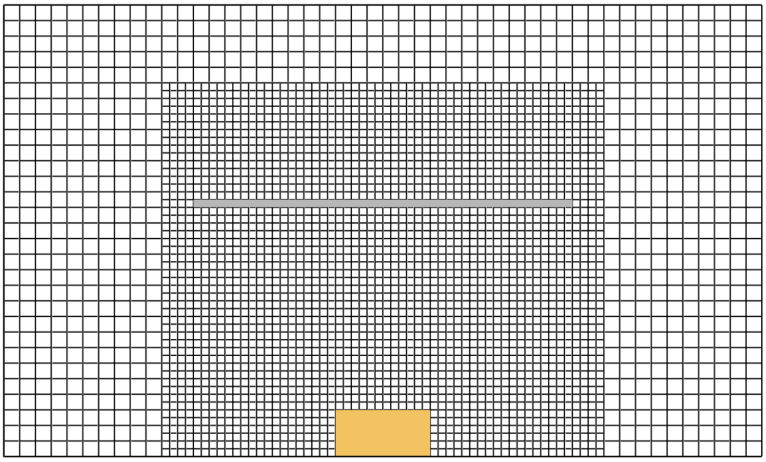

Figure 4: Hybrid mesh strategy in Wasson cases.

Figure 5 shows the ceiling temperature at the stagnation point at three resolutions for the Wasson experiments. Figure 5a shows the smallest fire with the largest ceiling, and Figure 5b shows the largest fire with the smallest ceiling. In both cases the 25 mm resolution was reasonably converged with the 12 mm model.

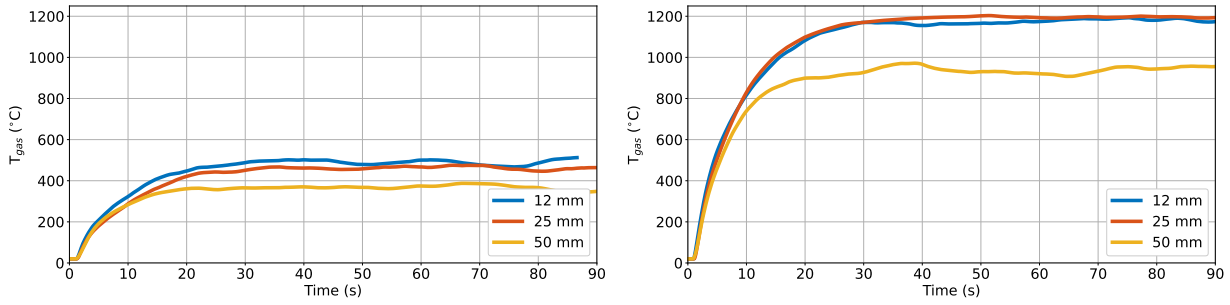

(a) Scenario 1, 50 kW, 0.97 m

(b) Scenario 6, 90 kW, 0.64 m

Figure 5: Ceiling temperature variability with grid resolution in Wasson cases.

One method to characterize the grid resolution of a buoyantly driven fire plume is to calculate the ratio of the characteristic fire diameter to the grid resolution [19],

$$D^* = \left(\frac{\dot{Q}}{\rho_\infty c_p T_\infty \sqrt{g}} \right)^{2/5} \approx \left(\frac{\dot{Q}}{1100} \right)^{0.4} \tag{7}$$

where D^* is the characteristic fire diameter, $\dot{Q}$ is the heat release rate in kW, and g is the acceleration due to gravity. A 25 mm resolution was used to model all cases in this work based on the grid convergence study which corresponds to a D^*/dx of 11-15 for the Wasson cases and 18-27 for the Lattimer cases.

The Lattimer corridor cases used a fixed grid resolution over the full domain. The mesh domain was extended 0.3 m in all directions except the floor which was not extended and the corridor exit which was extended 0.8 m to allow more room for smoke movement. The walls and ceiling of the enclosure were modeled as one grid cell thick.

Dynamic Pressure

The gas temperatures in the converged solution in Figure 5 were higher than those measured by Wasson. It is hypothesized that there was a slight tilt in the flame in the experiments due to ambient conditions. A small tilt can result in a large local temperature difference due to the high gradient in the stagnation region. A small ambient bias was introduced along one axis in the Wasson cases to simulate this effect. The bias was introduced by varying the dynamic pressure, p_{dyn}, at the open boundaries where

$$\begin{aligned} H &= p_{\text{dyn}}/\rho_\infty + |\mathbf{u}|^2/2 && \text{(outgoing)} \\ H &= p_{\text{dyn}}/\rho_\infty && \text{(incoming)} \end{aligned} \tag{8}$$

Figure 6 demonstrates the impact of different ambient biases on the temperature at the point gas temperatures were measured in the experiment. The dynamic pressure was converted in each case to an effective flow velocity using Eq. 8. Predictions from a sensitivity case with sinusoidal noise which varied from 80% of the peak value to 100% peak over a 10 second period are also shown in Figure 6. It was found that the ambient bias of 0.16 m/s without the sinusoidal noise agreed well with the experiments and was used in the simulations of the unconfined ceiling. No dynamic pressure was used in the Lattimer cases.

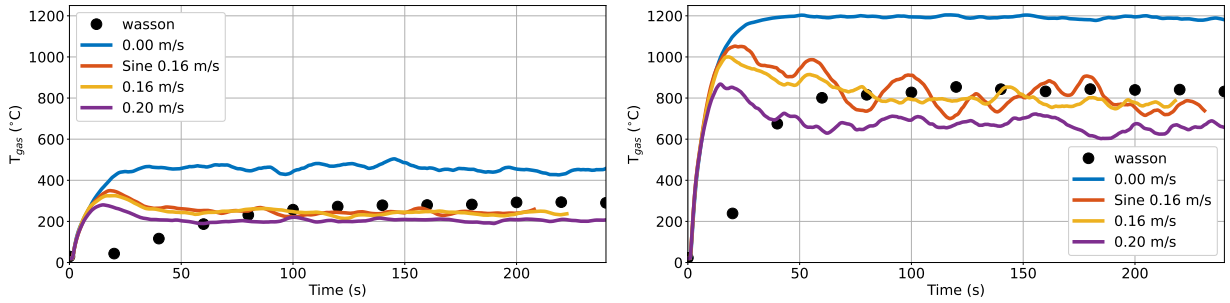

(a) Scenario 1, 50 kW, 0.97 m *(b) Scenario 6, 90 kW, 0.64 m*

Figure 6: Ceiling temperature variability with wind bias in Wasson cases.

Thermal Model

The thermal response of the structural elements to the heat transfer from the fire was calculated using the methodology outlined by Buchanan in [5]. The section temperature for an unprotected member is solved using an explicit time integration of the equation

$$\frac{dT_s}{dt} = \left(\frac{F}{V\rho_s c_{p,s}}\right) \cdot \left[h_c\left(T_f - T_s\right) + \sigma\varepsilon_r\left(T_f^4 - T_s^4\right)\right] \tag{9}$$

where T_s is the mean section temperature, F is the exposed surface area per unit length, V is the volume of steel per unit length, T_f is the exposure temperature, considered to be the adiabatic

surface temperature in this work, ε_r is the resultant emissivity, considered to be 0.7 as recommended by Buchanan, and the subscript s indicates properties for the steel. The specific heat of the steel is defined as a function of temperature in accordance with the American Institute of Steel Construction (AISC) guidance for 20 °C $\leq T_s \leq$ 600 °C, [1]

$$c_s = 425 + 0.773T_s - 1.69 \times 10^{-3}T_s^2 + 2.22 \times 10^{-6}T_s^3. \tag{10}$$

In this work, the exposure temperature is taken to be the adiabatic surface temperature (AST) which is the theoretical surface temperature at which the total heat flux is zero [28]. The AST can be calculated from the gauge heat flux using the equation

$$\varepsilon_g \sigma T_{AST}^4 + hT_{AST} + \left(-\varepsilon_g \sigma T_g^4 - hT_g - \dot{q}''_{tot,g}\right) = 0 \tag{11}$$

where T_{AST} is the adiabatic surface temperature, and T_g is the temperature of the gauge. Equation 11 can be solved analytically using the approach presented by Malendowski [17] where the coefficients of the polynomial are modified per Equation 11.

The exposed surface area per unit length is calculated assuming a three-sided exposure to a structural I-beam (i.e., the top of the member is not exposed to the fire). This is a typical representation of a beam supporting a concrete slab. The exposed perimeter is calculated assuming the two flanges and web are rectangles (i.e., neglecting rounded sections). The resulting equation for the F/V of a unit length is

$$\frac{F}{V} = \frac{3b_f + 2d - 2t_w}{2b_f t_f + (d - 2t_f)t_w} \tag{12}$$

where b_f is the flange width, d is the depth of the section, t_w is the thickness of the web, and t_f is the thickness of the flange. The structural member considered in this analysis is a W24x192 type which is typical of primary members in high rise construction, and has the dimensions defined in Table 3.

Table 3: Structural members analyzed in this study.

AISC Label	b_f (mm)	d (mm)	t_w (mm)	t_f (mm)	F/V (m)
W24x192	330	648	20.6	37.1	61.8

Uncertainty Statistics

The uncertainty statistics in this work are calculated using the approach presented in [23] which is also used in the FDS Validation Guide [21]. This approach decomposes the model uncertainty into a systematic bias factor, δ, and standard deviation, σ_M. Values of $\delta \approx 1$ demonstrate no systematic bias. Values less than 1 indicate the model has a tendency to underpredict the quantity, and values greater than 1 indicate the model tends to overpredict the quantity. Values of σ_M closer to zero indicate no spread in uncertainty across measurements after correcting for systematic bias.

RESULTS

Hot Jet

Figure 7 shows FDS results for three grid resolutions compared to the correlation in Martin [18, 3]. These results show that better agreement at the lower Re; however, the higher Re is still within

approximately 25% across a four times multiple in grid resolution. In each case the heat transfer coefficient is significantly higher than the values predicted using the default convection relationships in FDS. Figure 8 shows the profile of h along the ceiling. As expected, the highest heat transfer coefficient occurs at the stagnation point and drops as the flow traverses the ceiling.

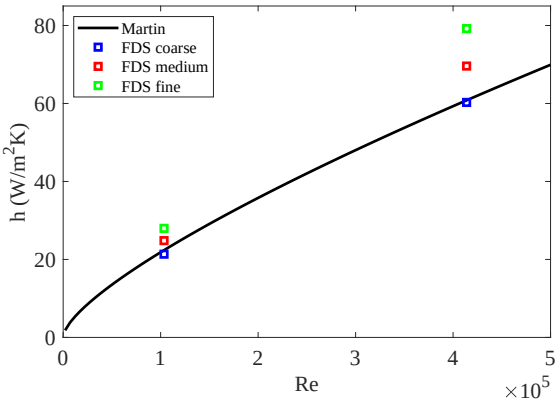

Figure 7: Average Nusselt number correlation for a flat plate compared to FDS results using the impinging jet heat transfer model.

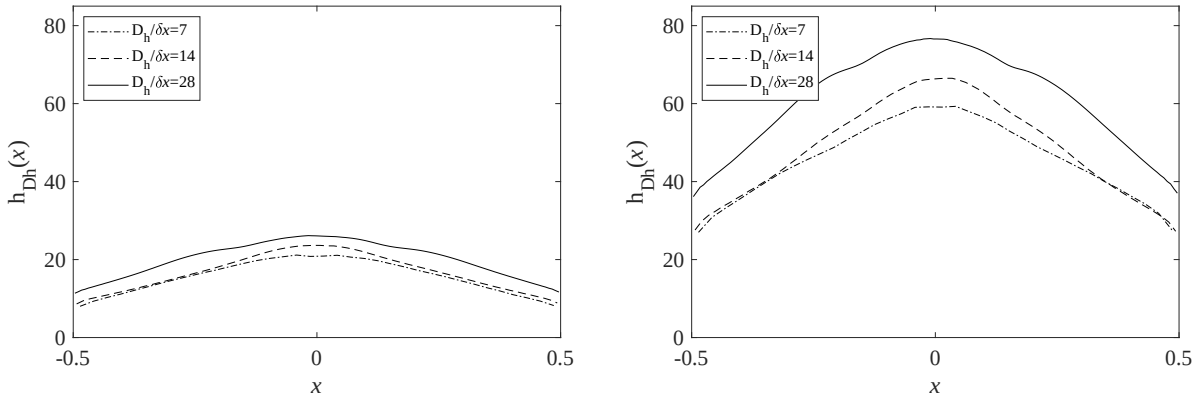

(a) Re=1 × 10⁵ *(b) Re=4 × 10⁵*

Figure 8: Profile of average Nusselt number (Nu) along the ceiling at Reynolds numbers (Re) based on jet diameter.

Fire Impinging on a Ceiling

The heat transfer coefficient predicted using the new impinging jet relationship for scenario 6 ($\dot{Q}$=90 kW, H=0.64 m) is shown in Fig. 9. There are two main differences observed in comparison with the default model shown in Fig. 1. The local minima at the stagnation point is no longer present with the impinging jet model, and the overall magnitude of the heat transfer coefficient is in line with the experimental measurements and engineering guidance on local fires.

Similar trends can be observed in the heat transfer coefficient at the stagnation point in each of the five cases shown in Fig. 10. As expected, the heat transfer coefficient using the default FDS convec-

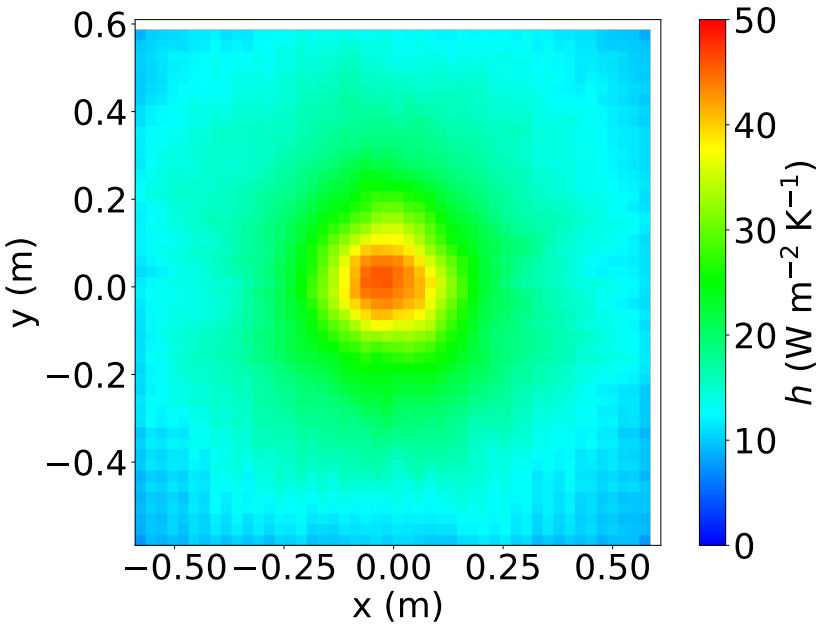

Figure 9: Heat transfer coefficient from a 90 kW fire impinging on a ceiling located 0.64 m above the fire using the impinging jet FDS convection configuration.

tion relationship is low across all six cases at approximately 6 W/(m^2 K) due to the low tangential velocity at the stagnation point. The impinging jet relationship agrees better with the experiments with values ranging from 25-50 W/(m^2 K). The black solid line shows the 1:1 line between the model and the experiments. The two dashed black lines show an estimated experimental uncertainty of 7.5%. The red solid line shows the systematic bias in model performance, and the two dashed red lines show a 95% confidence interval after correcting for the model bias. See McGrattan *et al.* for a discussion of the uncertainty calculation approach [23]. Note the experimental points in Fig. 10 were taken to be the steady-state average values after digitizing the data from Wasson rather than the tabular values which included a high transient heat flux during initial exposure.

Figure 11 presents a similar uncertainty comparison of the time-averaged gauge heat flux predicted using the default and impinging jet models with the measurements obtained by Wasson and Lattimer. The uncertainty statistics demonstrate that the default convection relationships in FDS generally underpredict the heat flux with a bias factor 0.65. The impinging jet relationship improves the statistical performance and changes the model to have a tendency to overpredict the heat flux with a bias of 1.09.

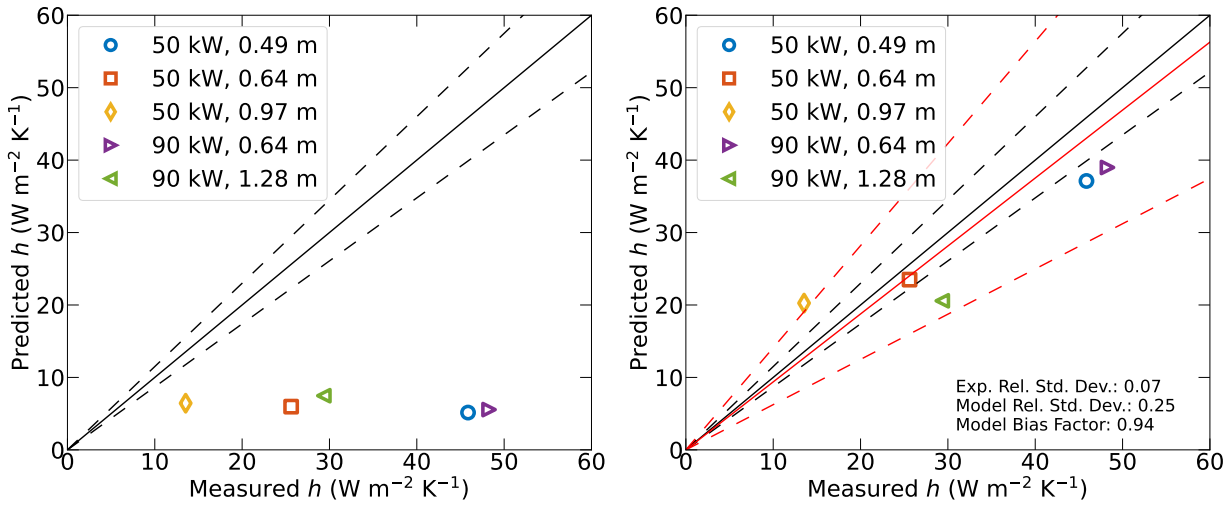

(a) FDS default, commit 5ac3c1c. *(b) FDS impinging jet.*

Figure 10: Stagnation point heat transfer coefficient in Wasson cases.

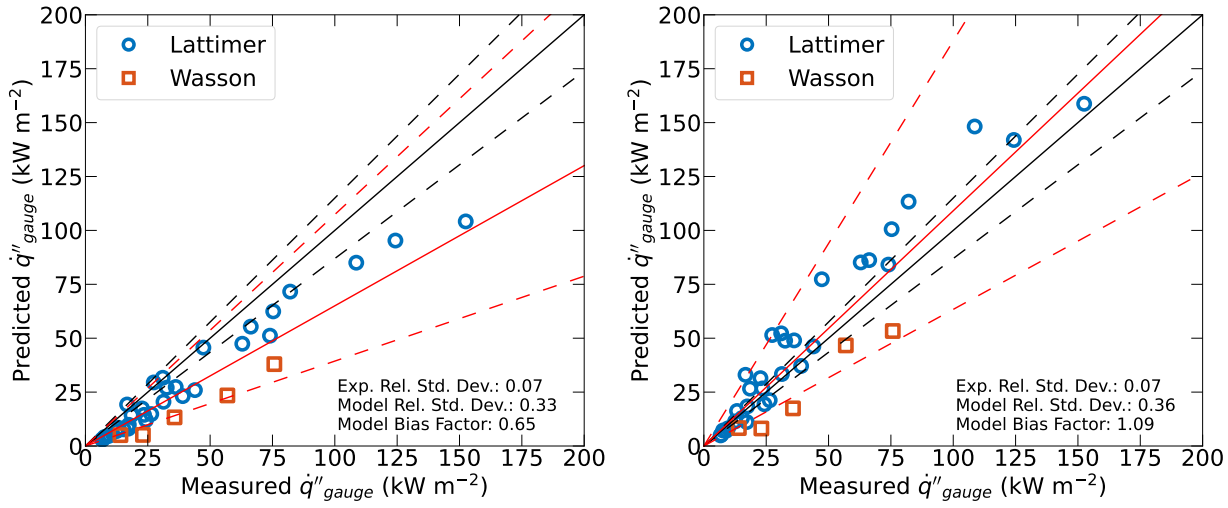

(a) FDS default, Wasson with commit 5ac3c1c. *(b) FDS impinging jet.*

Figure 11: Comparison of model-predicted and experimentally measured time-averaged gauge heat flux.

DISCUSSION

The heat flux predictions using the impinging jet model agrees better with the experimental measurements in both the unconfined ceiling and corridor ceiling configurations. The systematic bias across the two data sets is 1.09 indicating a slight tendency of FDS to overpredict the gauge heat flux with the impinging jet model. However, Figure 11b shows a slight systematic difference between the two sets of validation data where the Wasson dataset is generally below the 1:1 line with the experiments and the Lattimer dataset is generally above it. If the systematic bias is calculated separately for the two datasets, the Wasson set has a bias of 0.59, and the Lattimer set has a bias of 1.16, and both cases have a similar standard deviation of 0.28.

There are several potential sources of these differences. The burner used in the two experiments was quite different. Wasson used a square burner with a side length of 0.3 m; whereas, Lattimer used a rectangular burner with a non-unity aspect ratio which was 0.46 m deep and 1.15 m long. It is possible that the approach used to calculate the equal area diameter in the rectangular burner contributes to the difference between these two data sets. The two test series also used different sensors to measure the heat flux to the ceiling. Lattimer used a more typical water-cooled thermopile of Schmidt-Boelter type; whereas, Wasson used a custom designed high temperature heat flux sensor which was converted to an equivalent water-cooled heat flux in this work which relies on the heat transfer coefficient values measured by Wasson. Uncertainty in calculating h propagates to additional uncertainty in the experimental gauge heat flux measurements for this case.

In each case, the predicted heat fluxes are significantly higher than those predicted with the default convection model in FDS. As discussed in the performance-based design section, this could have a significant impact on analyses using FDS to evaluate the need for fire proofing on structure members. Figure 12 compares the section temperatures predicted by the lumped capacity model for a W24x192 member exposed to each of the eight corridor ceiling fires. In each case the steady temperature reached after a 3 hour exposure is 100-200 °C higher using the impinging jet model than the default convection model. While in most cases the member is predicted to have failed with both models, the top two scenarios in Figure 12 demonstrate the impact this can have on design. In these scenarios the impinging jet model predicts the member will reach the failure criteria, whereas the default convection model does not. A system which is designed using exposures predicted by the default convection model may fail prematurely if the real exposures are closer to those predicted by the impinging jet.

The initial validation results indicate the impinging jet model provides more accurate predictions of the heat flux; however, additional work is needed to verify these findings. The fire sizes and fire diameters included in this validation work are limited by the availability of data. The plumes developed by realistic fuel sources with complex geometry encountered infrastructure (e.g., foliage, upholstered furniture, etc.) may behave differently than the gas burners on which this study focused. Additional research is needed to better understand the heat fluxes to ceilings from these fuel sources, any modifications to Re coefficients for these fuel sources, and best practice guidance on how to select an appropriate length scale for the impinging jet model in these cases.

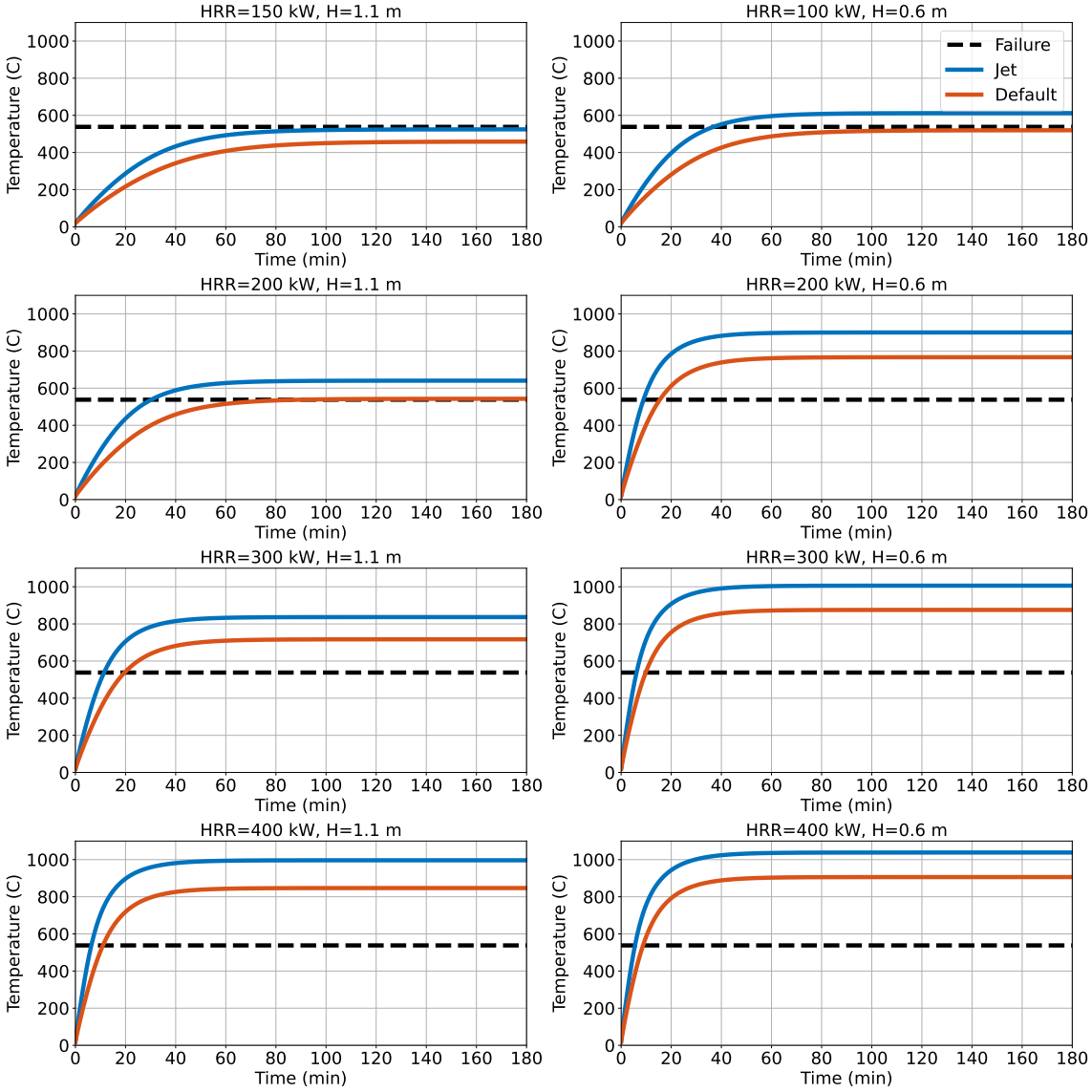

Figure 12: Impact of convective heat transfer model on predicted structural performance.

CONCLUSIONS

The recently implemented impinging jet model in FDS removes the fictitiously low heat transfer coefficient near the stagnation region. The initial validation presented in this paper indicates the model improves the predictions of heat fluxes to ceilings from gas burners compared to the default convection model in FDS. The systematic bias in heat flux predictions on the validation cases is fairly close to unity at 1.09; however, there are systematic differences observed in the statistical performance between the two data sets. It is possible that these differences are related to limitations in the model in considering non-unity fire sources, or that they are related to differences in experimental methods used by the authors.

While additional work is needed to expand the validation basis of this model, the initial results indicate that the impinging jet model is more accurate than the default convection relationships. Because the impinging jet model predicts higher thermal exposures than the default, the corresponding heat fluxes are generally higher. These results indicate that users of FDS may need to consider using the impinging jet model when using FDS to evaluate the need for structural fire proofing as the default convection model may provide a non-conservative estimate of the structural response.

REFERENCES

[1] ANSI/AISC. *Specification for structural steel buildings*. ANSI/AISC, 2016.
[2] ASTM International. *E119-24 Standard Test Methods for Fire Tests of Building Construction and Materials*. Tech. rep. ASTM International, 2024. DOI: 10.1520/E0119-24.
[3] T.L. Bergman et al. *Fundamentals of Heat and Mass Transfer*. 7th. New York: John Wiley and Sons, 2011.
[4] C. Beyler. "SFPE Handbook of Fire Protection Engineering". In: 5th. New York: Springer, 2016. Chap. Flammability Limits of Premixed and Diffusion Flames.
[5] Andrew H. Buchanan and Anthony K. Abu. *Structural Design for Fire Safety*. John Wiley & Sons, 2017. ISBN: 9780470972892. DOI: 10.1002/9781118700402.
[6] International Code Council. "Chapter 6 Types of Construction". In: *International Building Code*. International Code Council, 2024.
[7] International Code Council. "Chapter 7 Fire and Smoke Protection Features". In: *International Building Code*. International Code Council, 2024.
[8] T. E. Diller. "Heat Flux Measurement". In: *Mechanical Engineers' Handbook Volume 4 - Energy and Power*. Ed. by Myer Kutz. Fourth. Hoboken, New Jersey: Wiley, 2015. Chap. 7, pp. 1–27.
[9] Fiberfrax. *Fiberfrax Durablanket S*. Unifrax Engineering, Dec. 2009.
[10] Steven M.V. Gwynne and K.E. Boyce. "Engineering Data". In: *SFPE Handbook of Fire Protection Engineering, Fifth Edition*. Ed. by Morgan J. Hurley. SFPE, 2016.
[11] Y. Hasemi et al. "Fire Safety of Building Components Exposed to a Localized Fire". In: *Proceedings of the ASIAFLAM*. 1995, pp. 351–361.
[12] Simo Hostikka, Kevin B. McGrattan, and Anthony Hamins. "Numerical modeling of pool fires using LES and Finite Volume Method for radiation". In: *Fire Safety Science* M (2003), pp. 383–394. ISSN: 18174299. DOI: 10.3801/IAFSS.FSS.7-383.
[13] Yu Jeong Kim and Arnaud Trouvé. "Evaluation of angular resolution requirements in the finite-volume-method solution of the radiative transfer equation". In: *Fire Safety Journal* 141 (Dec. 2023). ISSN: 03797112. DOI: 10.1016/j.firesaf.2023.103971.

[14] Brian Y. Lattimer. "Heat Transfer from Fires to Surfaces". In: *SFPE Handbook of Fire Protection Engineering, Fifth Edition*. SFPE, 2016, pp. 745–798.

[15] Brian Y. Lattimer, Christopher Mealy, and Jesse Beitel. "Heat Fluxes and Flame Lengths from Fires Under Ceilings". In: *Fire Technology* 49 (2 2013), pp. 269–291. ISSN: 00152684. DOI: 10.1007/s10694-012-0261-1.

[16] J.N.B. Livingood and P. Hrycak. *Impingement Heat Transfer from Turbulent Air Jets to Flat Plates - A Literature Survey*. NASA Tehnical Memorandum. Washington, D.C.: National Aeronautics and Space Administration, 1973.

[17] M. Malendowski. "Analytical Solution for Adiabatic Surface Temperature (AST)". In: *Fire Technology* 53 (2017), pp. 413–420. DOI: 10.1007/s10694-016-0585-3.

[18] H. Martin. "Heat and Mass Transfer Between Impinging Gas Jets and Solid Surfaces". In: *Advances in Heat Transfer*. Ed. by J.P Hartnett and Jr. T.F. Irvine. Vol. 13. New York: Academic Press, 1977.

[19] Randall J Mcdermott. "Quality Assessment in the Fire Dynamics Simulator: a Bridge To Reliable Simulations". In: *Proceedings Fire and Evacuation Modeling Technical Conference*. 2011.

[20] K. McGrattan et al. *Fire Dynamics Simulator, Technical Reference Guide, Volume 1: Mathematical Model*. sixth. 1018-1. NIST Special Publication. National Institute of Standards, Technology, Gaithersburg, Maryland, USA, and VTT Technical Research Centre of Finland, Espoo, Finland. Sept. 2013.

[21] K. McGrattan et al. *Fire Dynamics Simulator, Technical Reference Guide, Volume 3: Validation*. sixth. 1018-3. NIST Special Publication. National Institute of Standards, Technology, Gaithersburg, Maryland, USA, and VTT Technical Research Centre of Finland, Espoo, Finland. Sept. 2013.

[22] K. McGrattan et al. *Fire Dynamics Simulator, User's Guide*. sixth. 1019. NIST Special Publication. National Institute of Standards, Technology, Gaithersburg, Maryland, USA, and VTT Technical Research Centre of Finland, Espoo, Finland. Sept. 2013.

[23] Kevin McGrattan and Blaza Toman. "Quantifying the predictive uncertainty of complex numerical models". In: *Metrologia* 48 (3 2011), pp. 173–180. ISSN: 00261394. DOI: 10.1088/0026-1394/48/3/011.

[24] SFPE. "Appendix 3: Fuel Properties and Combustion Data". In: *SFPE Handbook of Fire Protection Engineering, Fifth Edition*. SFPE, 2016.

[25] SFPE. *Engineering Guide Fire Exposures to Structural Elements*. 2004.

[26] Underwriters Laboratory. *UL 263 Standard for Fire Tests of Building Construction and Materials*. Tech. rep. Underwriters Laboratory, 2024. DOI: 10.1520/E0119-24.

[27] Rachel Wasson. "Separation of the Heat Transfer Components from Diffusion Flames Impinging onto Ceilings". PhD thesis. Virginia Tech, 2014.

[28] U. Wickström, D. Duthinh, and K.B. McGrattan. "Adiabatic Surface Temperature for Calculating Heat Transfer to Fire Exposed Structures". In: *Proceedings of the Eleventh International Interflam Conference*. Interscience Communications, London, 2007.

[29] G. Zhou. "Numerical simulations of physical discontinuities in single and multi-fluid flows for arbitrary Mach numbers". PhD thesis. Goteborg, Sweden: Chalmers Univ. of Tech., 1995.